Department of Veterans Affairs

Journal of Rehabilitation Research and Development Vol. 33 No. 3, July 1996
Pages 239–252

Indentor tests and finite element modeling of bulk muscular tissue in vivo

William M. Vannah, PhD and Dudley S. Childress, PhD
Rehabilitation Engineering Program, Northwestern University Chicago, IL 60611

Abstract—The quasi-static response of bulk muscular tissue to indentation was measured on the posterior lower legs of living human subjects. No residual limbs were tested; all subjects had intact lower limbs. For loads up to 7.0 N on an 8.0 mm diameter flat-tipped indentor, the response was repeatable without prior 'preconditioning.' The data at any test location exhibited substantial random scatter, but did not trend up or down with repeated cycles. At these limited loads (<7.0 N), hysteresis was always evident but was always ≤10% of the maximum reaction force generated. At these limited loads, stress relaxation, in the time period between 5 and 1200 seconds after indentation, was <10% (>90% confidence). At higher load levels (>12.0 N), greater hysteresis and prolonged stress relaxation were observed, accompanied by minor tissue damage.

In order to estimate the composite material stiffness of the tissue, the indentations were modeled using a materially and geometrically nonlinear, large-strain finite element formulation. The resulting composite material stiffness was nonlinear, and could be approximated using the Jamus-Green-Simpson strain energy function; typical values for the coefficients were c_{10}=0.0026 MPa, c_{01}=0.00064 MPa, and c_{11}=0.0057 MPa.

Key words: *artificial limbs, biomechanics, elasticity, pressure sores, prosthetic fitting, soft tissue, tissue response.*

This material is based upon work supported by the National Institutes on Disability and Rehabilitation Research and by the New England Medical Center Hospitals.
Address all correspondence and requests for reprints to: William M. Vannah, PhD, Shriners Hospital, Springfield Unit, 516 Carew Street, Springfield, MA 01104; email: wvannah@aol.com.

INTRODUCTION

Data describing the behavior of bulk muscular tissue under contact loads are necessary in mechanical analyses of prosthetic sockets, custom wheelchair seating, and other soft tissue support devices for the disabled. Historically, a majority of these analyses have used a static, linearly elastic material model; although nonlinear, viscoelastic behavior has been reported in soft tissues (1–7). A static, linearly elastic model of the stresses in a soft solid at the interface between a hard and soft solid, developed for analysis of foundations built on marginal soils (8), was applied to soft tissues by Murphy and Bennett to estimate the stress distribution under orthoses (9,10). Chow and Odell analyzed wheelchair seating stresses using a static, geometrically nonlinear model (11). Nakamura et al. used a static, materially and geometrically nonlinear model for cadaver heel tissue, calculating modulii from 0.5 to 7 MPa (12). Krouskop et al. used indentor tests of above-knee residua, and a static, linearly elastic model to derive elastic modulii of 0.0062, 0.036, and 0.109 MPa for relaxed muscle, mild isometric activity, and maximum isometric activity, respectively (13). Steege et al. used indentor tests of below-knee residua and a static, linearly elastic model to derive an elastic modulus of 0.06 MPa (14). Steege and Childress later used a geometrically and materially nonlinear model, with some improvement noted in the correlation between observed and calculated interface pressures (15). Reynolds used indentor tests of intact (i.e., non-amputated) legs and a static, linearly elastic model to derive elastic modulii in the range 0.050 to 0.145 MPa

(16). Mak et al. used indentor tests of residua and intact limbs and a static, linearly elastic model, calculating modulii from 0.021 to 0.195 MPa (6). Other investigators have performed analyses of the mechanics of soft tissue support using a linear elastic material model, and material properties from the literature (5,7,17).

More complex material models have been used for soft tissue mechanics in other fields; relevant examples could include the following. The behavior of *in vivo* and *in vitro* skeletal muscle has been studied extensively (18). This work generally has used one-dimensional line models with spring and damper elements; viscoelasticity and nonlinear stiffness have been included in the material model. Multidimensional continuum models have been developed for *in vivo* and *in vitro* cardiac muscle. Material models used in this area of research commonly have included nonlinear stiffness and geometric effects, but have assumed negligible viscoelasticity (19–22). The biphasic material model for articular cartilage reproduces this tissue's pronounced viscoelastic behavior by postulating a liquid phase, whose time rate of passage through a postulated solid phase depends on the pressure gradient, the dilatation of the solid phase, and other factors (1,4,23). Nonlinear stiffness has been included in this model. Oomens and co-workers employed a similar biphasic model in their indentor studies of *in vitro* porcine skin and subcutaneous fat (24). The response of *in vivo* skin to uniaxial tension was modeled by Manshot and Brakkee; this model included nonlinear stiffness and viscoelasticity (25).

Thus, material and geometric nonlinearities and viscoelasticity have been included in mechanical analyses of a number of soft tissues. However, these nonlinearities and viscoelasticity have not been commonly included in analyses of bulk muscular tissue, at least not in soft tissue support problems within rehabilitation engineering, although these behaviors have been observed. In order to determine whether material stiffness nonlinearity and viscoelasticity are appropriate inclusions in a given soft tissue support problem, quantitative description of these material behaviors is necessary.

Objective

The objective of the study was to provide a quantitative description of the material stiffness nonlinearity and viscoelasticity occurring in bulk muscular tissue, under loads such that the data may be used in soft tissue support problems within rehabilitation engineering. The study was limited to experimental recording of the quasi-static response of the tissue; specifically, the response over the time period from 60 to 1,200 seconds after displacement imposition. As an integral part of the description of the material nonlinearity, a typical nonlinear composite material stiffness was estimated, assuming a homogeneous isotropic material model.

METHODS

Subjects

All subjects had intact lower limbs; that is, no residual limbs were tested. One 30-year-old male subject was used for the bulk of the tests. An abbreviated series of tests was conducted using seven subjects; two females and five males, 21 to 33 years of age, with weights ranging from 115 to 195 lbs (52.16 to 88.45 kg).

Experimental

A high distortion indentor test was chosen to deform the tissue. Indentor tests have been used by a number of investigators studying soft tissue support, both for quantification of tissue properties (6,14–16,26), and directly for the design of soft tissue support devices (17,27,28). Because high distortions were to be used, which might compromise the health of a residual limb, testing was instead conducted on humans with intact legs. The rationale for applying large distortions is that, in general, higher distortions cause bulk muscular tissue to exhibit increased inelasticity, and it was desired to explore a larger range of distortion than that anticipated clinically (i.e., to overpredict inelasticity); therefore, high distortion tests were used.

Apparatus

In vivo indentor tests were performed on the calf (posterior muscle belly) of the lower leg. The stiffness of the calf was measured using the tissue tester, a device consisting of an indentor with a linear variable differential transformer (LVDT) and a load cell (**Figure 1**), which measured applied displacement and resulting force simultaneously (14). Flat-tipped, cylindrical indentors of either 8.0 or 19.0 mm diameter were used. Indentation was normal to the surface of the tissue.

A custom fixation device was created to hold the tissue tester in position over the muscle belly (**Figure 2**. Two goals were specified in the design of the fixation device. First, the device should hold the tissue tester

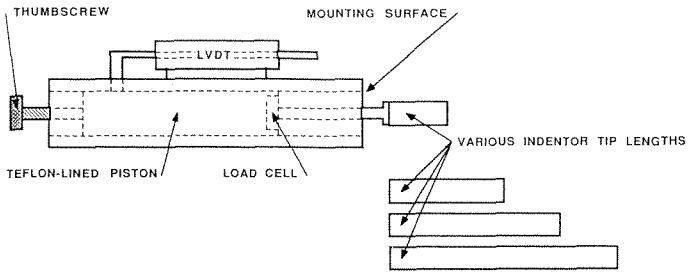

Figure 1.
The tissue tester. This device consisted of an indentor with a load cell and an LVDT. The range of the LVDT was limited to 10.0 mm, in order to allow a larger range of indentations; a number of different length indentor tips were used.

immobile relative to the underlying bony structure of the legs. Secondly, the device should not impede the free motion of the calf tissue. It is simpler to model the mechanics of a body whose boundaries are either fully free to move, or fully prevented from motion. Boundary conditions between those extremes (e.g., those that change during loading) are more complex to model. Considerable attention was paid to ensuring that the device did not slip (shear) along the skin, thus falsely recording viscoelasticity. Dry friction, between the skin and a boundary wall, might have caused behavior which could have been mistaken for material inelasticity. For instance, if the skin were drawn (slipped) along a boundary wall during an indentation, then did not return as the indentation was removed, the force-displacement curve might have exhibited what appeared to be viscoelasticity, even if the material itself were not viscoelastic.

The fixation device was completely external to the body, clamping about the bony prominences of the knee, tibial crest, and malleoli. A shell was constructed by vacuum-forming a 3/16-in (4.76 mm) thick polypropylene sheet around a plaster mold of the subject's leg. The majority of this shell was then cut away, so that the remainder cupped the lateral and medial malleoli, contacted the length of the tibial crest, and cupped the lateral and medial aspects of the tibial plateau. Otherwise, the remaining shell did not touch the leg anywhere; thus, minimally impeding free displacement of the muscle belly. Ears were added to the posterior aspect of the shell (**Figure 2**), and the shell was clamped to a wooden backbone using these ears. The backbone served to stiffen the shell and functioned as a mounting area for the tissue tester. The backbone did not contact the leg.

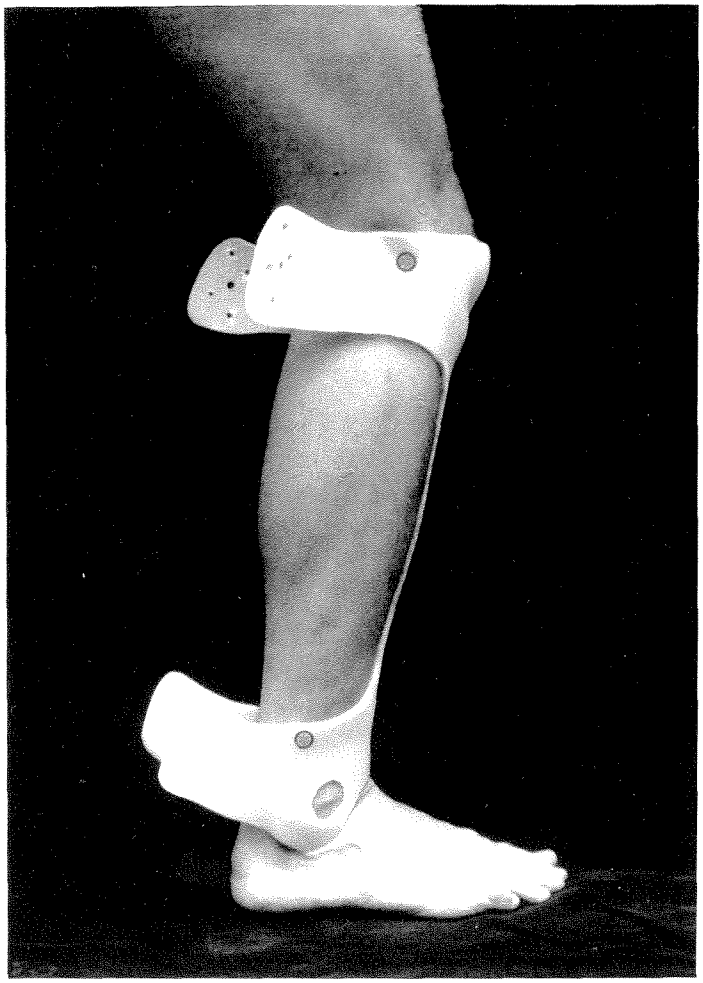

Figure 2.
The attachment portion of the fixation device, the 'shell,' clamped to the leg about the malleolii and the medial and lateral aspects of tibial plateau; it was otherwise trimmed so that it minimally impeded the free motion of the soft tissues. The four ears of the shell were clamped to a wooden backbone. This backbone served to further stiffen the shell, and acted as a mounting surface for the tissue tester. Six test locations were used, arranged in two columns over the medial and lateral heads of the gastrocnemius.

Construction of the final shell involved multiple iterations on the mold shape (analogous to prosthetic socket rectification) in order to achieve a very tight fit without damaging tissue. With the first few mold shapes, the shell was a smaller circumference than that of the leg, that is, the shell was too tight when clamped. After clamping, the bony prominences over which the skin was unduly stressed (bruised, numb, excessively painful) were noted. The mold of the leg was then built up slightly in the area of these bony prominences, so that corresponding reliefs would be present in the next shell formed on the mold. This process was iterated

until a satisfactory fit was achieved. The mold was also modified so that the shell intruded in on the posterior aspects of the lateral and medial tibial plateau, and on the sides of the patellar tendon. The objective was to create a "bony lock" about the lateral and medial malleoli and the lateral and medial aspects of the tibial plateau, in as rigid a manner as possible. The shell appeared quite immobile relative to the underlying bone; however, no objective test was performed to quantify what level of slip did occur.

The wooden backbone of the fixation device, which clamped the shell closed, also served to hold a plastic surface for the tissue tester mounting flanges. Six aluminum mounting flanges were arranged in two columns, 4.0 cm apart over the medial and lateral heads of the gastrocnemius. Within each column, flanges were located at three heights; 8.0, 14.0, and 20.0 cm below the level of the tibial plateau. These flanges were aligned on the plastic surface so that indentation was normal to the surface of the leg.

All tests were conducted with the subject seated, and the knee and ankle angles held constant. Two levels of muscle activity were used: "relaxed" and "mild exertion," the latter defined as an isometric dorsiflexion against a force equal to 8 percent of body weight applied at the ball of the foot. Because the shell fabrication procedure was very demanding of the subject's time—and, essentially, could only be done by the subject—a fixation device was made for one subject only. Multisubject tests, using a different fixture, are described below.

Displacement-force Tests

The indentor tip was displaced in a quasi-static manner. The indentor was defined to have seated when the measured force exceeded 0.2 N. The indentor was threaded to a given position; then that position was held for 60 seconds before the resulting resistive force was recorded. The rest time of 60 seconds was chosen in order to allow short-term stress relaxation to occur before the reaction force was recorded. Further indentations were imposed, in a stepwise manner, until the reaction force exceeded 7.0 N. The indentor was then backed out, again in a stepwise manner, and the resulting reaction forces were similarly recorded. The time taken in threading the indentor to a new position was ~5 seconds, and was not controlled. The time between recording a force and stepping to a new indentation was also not controlled. Quasi-static loading is an attempt to duplicate a load history which has been commonly applied in CAD/CAM of soft tissue support devices. In a number of CAD/CAM methods (17,27,28), and in studies of socket interface pressures (14,15), the subject has rested on a soft tissue support device while various data were recorded at the soft tissue interface.

Because the displacement range required in order to generate 7.0 N (up to 30 mm) exceeded the range of the LVDT (10 mm), a set of indentor tips of various lengths was used (**Figure 1**). Thus, the tissue tester had to be dismounted from the fixation device in order to change to a different length indentor tip. Consequently, the resulting data formed a sequential set of points, one set of points for each indentor tip. These sets of points, somewhat overlapping, were then plotted on a common pair of axes forming a complete displacement-force curve (**Figure 3**). The time taken in changing the indentor tip (~15 seconds) was not controlled.

Using the relaxed and mild exertion conditions, the displacement-force relationship was measured in a stepwise manner at each of the six test locations, or ports. For the ports which were identified as the low (port II) and high (ports V and VI) stiffness ports, the measurement was repeated three times.

Twenty-minute Stress Relaxation Tests

Sufficient indentation to produce 5.0 N resistive force was imposed; this displacement was then main-

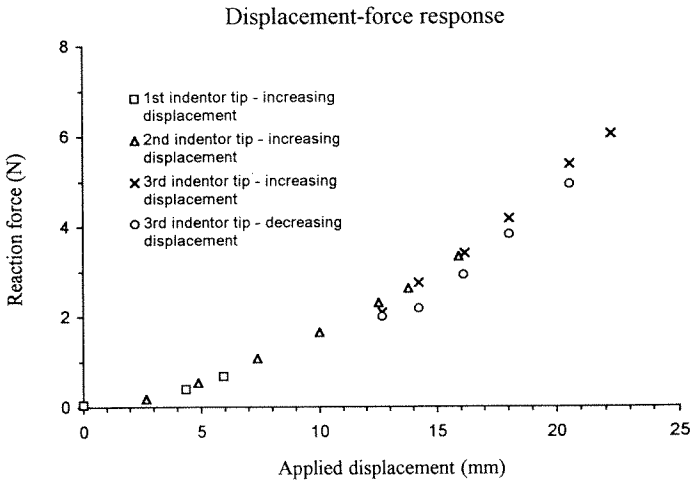

Figure 3.
Typical stepwise displacement-force response. The response when the three different length indentors are driven into the tissue (increasing displacement) forms a reasonably congruent composite curve. In contrast, the response when the indentor was removed from the tissue (decreasing displacement) shows clearly evident hysteresis.

tained for 1,200 seconds, and the resulting force profile over the time 5 to 1,200 seconds was recorded. Six trials were conducted, all with relaxed muscle, using various locations and indentor sizes. Stress relaxation tests were not successful for the mild exertion condition, nor for tests over 1,200 seconds in length; in both cases motions of the muscle belly occurred, effectively changing the applied displacement and invalidating the test.

Hysteresis Tests

The indentor was threaded in to 7.9 mm total displacement, then the applied displacement was cycled back and forth seven times between 7.9 and 12.8 mm. At each new displacement, rest times of 5, 10, 30, and 60 seconds were allowed to elapse before the resulting resistive force was recorded. All tests were at the 44.0 N activity level, location V.

Multisubject Tests

A test series was conducted to estimate the variation in tissue stiffness, variation from person to person, and with and without muscular exertion. In order to hold the lower leg motionless, a chair was built which supported the subject by the feet, knees, and buttocks following the so-called "Scandinavian office chair" design (**Figure 4**). An adjustable arm to hold the tissue tester was attached to the main trunk of the chair. The chair did not achieve the close-fitting bony lock of the shell device, and therefore could not be used for formal testing of inelasticities. Each subject was tested with the indentor tip located 65 percent of the distance up from the lateral malleoli to the tibial plateau, and 2.5 cm laterally out from the estimated centerline of the leg. The footrest of the chair was adjusted up or down according to the subject's leg length, so that the knee angle was the same for all subjects. The stiffness of the right leg of each subject was tested with the leg relaxed, and with the foot dorsiflexing against a resistance of 8 percent of body weight.

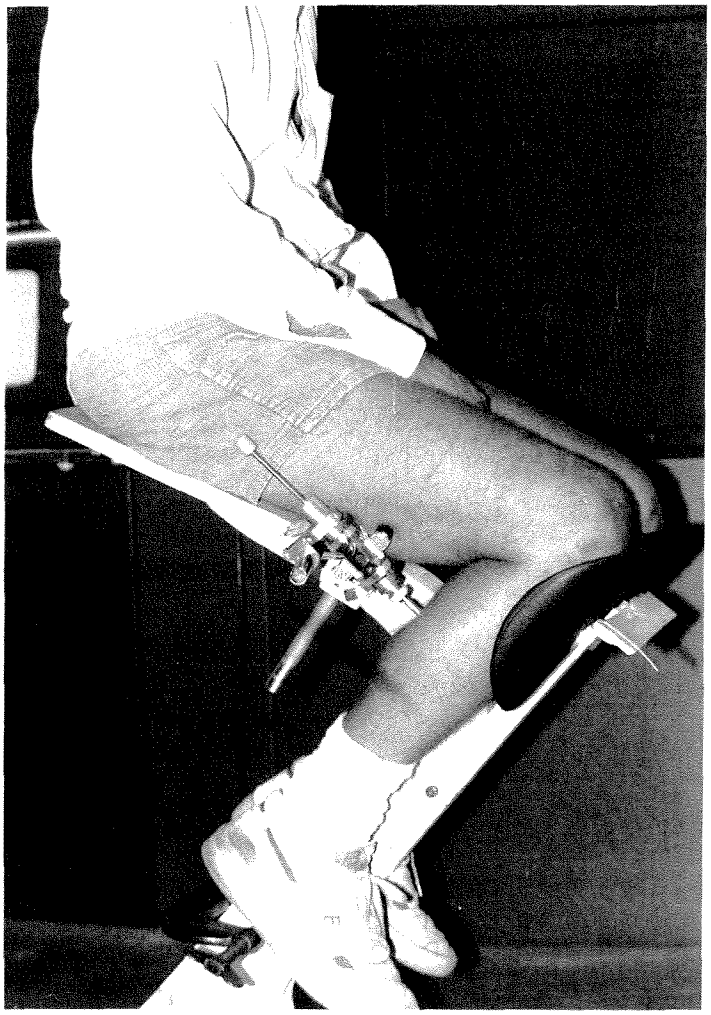

Figure 4.
The chair used for multisubject tests supported the subject at the buttocks, knees, and feet.

Finite Element Modeling

A finite element analysis of the indentation problem was used to calculate the nonlinear composite material stiffness. A novel feature of this analysis, relative to the previous use of indentor tests to estimate the stiffness of bulk muscular tissue, was that the global and local geometries of deformation were modeled in detail (6,14,16,26).

The mesh of the leg was constructed as follows: the internal and external geometry of the leg, from the tibial plateau to just above the malleoli, was recorded using a CT scan with horizontal cuts at 20 mm intervals (this interval allowed elements with adequate aspect ratios); the fixation device was worn during the scans, so that the coordinate frames of the radiographs and the fixation device could be referenced; the tibia and fibula were assumed rigid in comparison to the bulk muscular tissue, and so were left out and modeled by nodal constraints. From this general model of the leg, models were made with a more concentrated mesh incorporated at various indentation sites (**Figure 5**).

Linear elastic solutions for flat-tipped indentor contact problems show a singularity about the edge of the indentor (29). Modeling of this strong gradient was

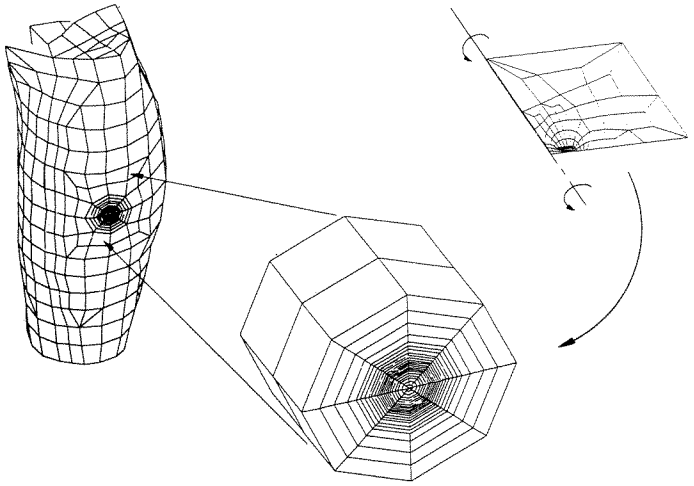

Figure 5.
Generation of an indentation model. The 2D axisymmetric model, developed as described in the appendix, was rotated through 360°; the resulting solid cylinder was inserted into the general leg model. In the case shown here, the cylinder is inserted so as to model indentation at test location IV. The general leg model was made by digitizing CAT scan slices. Before the refined mesh for indentation was added at any location, the model consisted of 982 eight-noded solid elements. The tibia and fibula were assumed rigid in comparison to the fleshy tissues and thus were left out and modeled by nodal constraints.

presumed to be the most severe constraint on the mesh design. An axisymmetric linear model of an indented layer was used in a procedure, based on the strain gradient, to find those areas most requiring mesh refinement (30). The resulting mesh (**Figure 5**) performed 3 percent more stiffly than a corresponding analytical solution (29). No analytical solution existed to verify the mesh and incremental scheme for the nonlinear model. Therefore, a parallel experimental test was conducted using a material with known properties.

Determination of Mesh Requirements and Interative Scheme for Nonlinear, Large-strain Modeling of the Indentor Problem

An artificial material, whose properties could be determined by independent tests, was deformed in the same manner as the finite element model, and results of experiment and model were compared. The material chosen was a mold-making silicone rubber (HSII®, Dow-Corning Corp., Midland, MI), chosen based on its ability to undergo very high elastic distortion without degradation. The properties of the HSII were determined using uniaxial tests; two samples in compression and one in tension (30). To describe the material's stiffness, the Jamus-Green-Simpson strain energy function was used (31–33):

$$W = c_{10}(I_1-3)+c_{01}(I_2-3)+c_{11}(I_1-3)$$
$$(I_2-3)+c_{20}(I_1-3)^2+c_{30}(I_1-3)^2$$

where the invariants, expressed in terms of stretch ratios (in place of strains), are:

$$I_1 = \lambda_1^2 + \lambda_2^2 + \lambda_3^2$$
$$I_2 = \lambda_1^2\lambda_2^2 + \lambda_2^2\lambda_3^2 + \lambda_3^2\lambda_1^2$$

and the stretch ratio is defined λ=deformed length/original length. The ratio of bulk to shear modulus is high enough for this material that we may assume the deformation is volume-conserving, thus:

$$I_3 = \lambda_1^2\lambda_2^2\lambda_3^2 = 1.$$

For uniaxial stretch in the '1' direction:

$$\lambda_1 = \lambda, \lambda_2 = \lambda_3 = \frac{1}{\sqrt{\lambda}}.$$

Substituting for λ_1, λ_2, and λ_3 in the Jamus-Green-Simpson potential function:

$$W = c_{10}(\lambda^2+\frac{2}{\lambda}-3)+c_{01}(2\lambda+\frac{1}{\lambda^2}-3)+c_{11}(\lambda^2+\frac{2}{\lambda}-3)$$
$$(2\lambda+\frac{1}{\lambda^2}-3)+c_{20}(\lambda^2+\frac{2}{\lambda}-3)^2 + c_{30}(\lambda^2+\frac{2}{\lambda}-3)^3$$

Solving this expression for the stress as a function of the stretch ratio:

$$\sigma = \lambda\frac{\delta W}{\delta\lambda}=2c_{10}(\lambda^2-\frac{1}{\lambda})+2c_{01}(\lambda-\frac{1}{\lambda^2})+$$
$$6c_{11}(\lambda^3-\lambda^2-\lambda+\frac{1}{\lambda}+\frac{1}{\lambda^2}-\frac{1}{\lambda^3})+$$
$$4c_{20}(\lambda^4-3\lambda^2+\lambda+\frac{3}{\lambda}-\frac{2}{\lambda^2})+$$
$$6c_{30}(\lambda^6-6\lambda^4+3\lambda^3+9\lambda^2-6\lambda-\frac{9}{\lambda}+\frac{12}{\lambda^2}-\frac{4}{\lambda^3})$$

We can then substitute x_1, x_2, x_3, x_4, and x_5, for the expressions in parentheses,

$$\sigma = c_{10}x_1+c_{01}x_2+c_{11}x_3+c_{20}x_4+c_{30}x_5$$

and use a linear, least-squares regression to determine c_{10} through c_{30}, given in **Table 1** (34). The material constants chosen were c_{10}=0.0457 MPa and c_{01}=0.0221 MPa (r^2=0.998). "Linear, least-squares regression" in this context refers to the calculated stress' linear dependence on the constants c_{10} through c_{30}; the functions of the stretch ratio, x_1 through x_5, are obviously nonlinear. This technique is sometimes referred to as a multiple regression.

Following determination of material constants by uniaxial test, the disk samples were then tested by the indentor method. Each sample was indented with 8.0 and 19.0 mm diameter flat-tipped indentors. These indentors had 150-grit sandpaper bonded to their tips in order to produce a zero-slip condition. The other end of the sample rested on a polished aluminum disk, and was coated with liquid soap, producing a zero-shear-stress condition.

Using the material constants from the uniaxial test, the finite element mesh was then tested to determine how well it would simulate the indentation tests. The Jamus-Green-Simpson strain energy potential function was employed; along with a mixed-field, stretch-ratio-based finite element solution formulation (35,36). This method was geometrically and materially nonlinear, and was general for large strains. The results of the simulation are shown in **Figure 6.** The finite element models match the experimentally measured initial stiffness very closely. At high indentations, the models behave somewhat more stiffly. The 8.0 mm model has a maximum error of 8 percent, occurring at 10.0 mm applied displacement. The 19.0 mm model has a maximum error of 12 percent at 22.0 mm displacement. These overpredictions may be, in part, due to partial tearing of the material. The disks showed a circle of minute pits, of the same diameter as the indentor used (i.e., either 8.0 mm or 19.0 mm). These pits indicate that the deformation was not fully elastic. The 8.0 mm indentor simulation was able to progress to 13.0 mm; after that point the solution became unstable. The 19.0 mm simulation was less severe on the material, and was able to progress further. Testing of a second sample produced similar results in all respects (30).

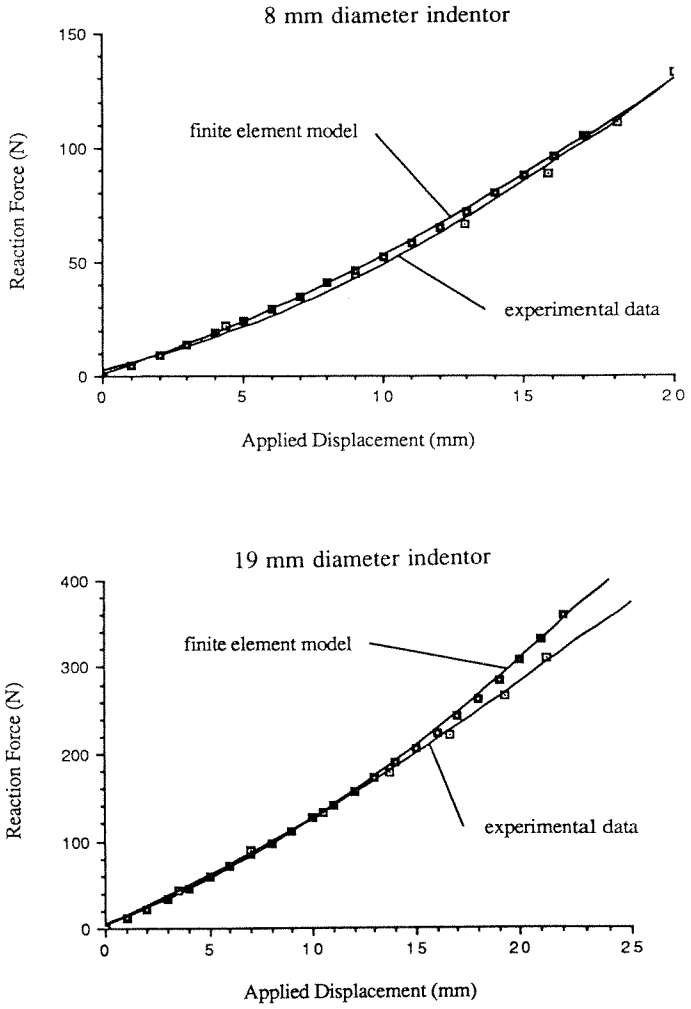

Figure 6.
Performance of elastomeric finite element indentor model in matching experimental response. The experimental data is from indentor tests upon silicon rubber disks. The material properties used in the finite element models of the indentations were determined from uniaxial compressive and tensile tests of same material.

Table 1.
Jamus-Green-Simpson coefficients for modeling response of HSII elastomer.

Coefficients Used	Best-fitting value of coefficient (Mpa) (and closeness of fit)
c_{10} only	0.0712 (r^2 = 0.97)
c_{01} only	0.0550 (r^2 = 0.93)
c_{10} and c_{01}	0.0457 (r^2 = 0.998) 0.0221
c_{10} and c_{11}	0.0592 (r^2 = 0.985) 0.0081
c_{10} and c_{20}	0.0683 (r^2 = 0.97) 0.0023
c_{10} and c_{30}	0.0680 (r^2 = 0.93) 0.0023

The most efficient incrementation scheme was found to be manually controlled 1.0 mm indentation steps. Within each increment, the method iterated until the residual energy (the energy stored in the structure calculated with old stiffness minus that calculated with new stiffness) was $\leq$10 percent of the energy at the old stiffness level.

The two-dimensional axisymmetric mesh thus developed and verified was converted to three dimensions by rotating it through 360° and incorporated into the general leg model at various indentation sites. The procedure of incorporating the concentrated mesh into the general model is shown graphically in **Figure 5.**

All modeling used the MARC/MENTAT finite element package (Marc Analysis Research Corp., Palo Alto, CA), installed on a Sun 3/260 computer. Two solution methods are reported here, with the following material models and solution formulations. The first method assumed a single homogeneous material and linear elasticity, using an element with a linear shape function and a reduced integration scheme (36,37). Poisson's ratio, ν, was equal to 0.499. The reduced integration scheme allows use of ν arbitrarily close, but not equal, to 0.50. For this model geometry, Poisson's ratio equal to 0.499 was verified to be sufficiently close to 0.50 to produce essentially identical results (30). The second method assumed a single homogeneous material, and used a large-deformation, materially and geometrically nonlinear solution. The element had a linear shape function and used the mixed-field formulation and Jamus-Green-Simpson material model previously described.

Constraint was applied by fixing all nodes at the interior surfaces of the tibia and fibula (i.e., modeling the bone as immobile and rigid). An analysis of the effects of this simplification is presented elsewhere (30).

Specifically, the leg models were: 1) Linear. Linear models were used with concentrated mesh at the ports identified in experimental testing as the low (II) and high (V and VI) stiffness ports. This set of models was used to test whether or not the stiffness variation at the ports was primarily a function of the geometry of the leg. 2) Nonlinear. Nonlinear models were used with concentrated mesh at the medium stiffness ports (III and IV). These models were used to estimate the composite material stiffness of the tissue. Due to excessive problem size, it was necessary to assume a horizontal plane of symmetry through the indentation (i.e., only half the leg was actually modeled). This assumption reduced the solution bandwidth (memory requirement) by a factor of eight. However, it also implicitly assumed that the displacement field was 1) immobile in the vertical direction everywhere on the symmetry plane and 2) was a mirror image about the symmetry plane. The effects of the first assumption were examined; the effects of the second were not examined (30).

RESULTS

Experimental Results

Displacement-force Tests

The typical displacement-force response (**Figures 3** and **7**) was smoothly varying, nonlinear, and consistently exhibited hysteresis. The ascending or descending portion of these data could be best fit with a parabolic regression. Of note was the minimal slope at low deformations: the slope of the curve at 2.0 mm is one-fifth of that at 20.0 mm.

Aside from this random variation, the muscle belly appeared to exhibit repeatable behavior without having to be "preconditioned" (2,3); that is, the stiffness did not trend up or down with repeated tests (**Figure 7**). Examples of displacement-force behavior with repeated cycles, for various locations and muscle activity levels, have been presented elsewhere (30). The data show a substantial amount of random variation. Uncontrollable

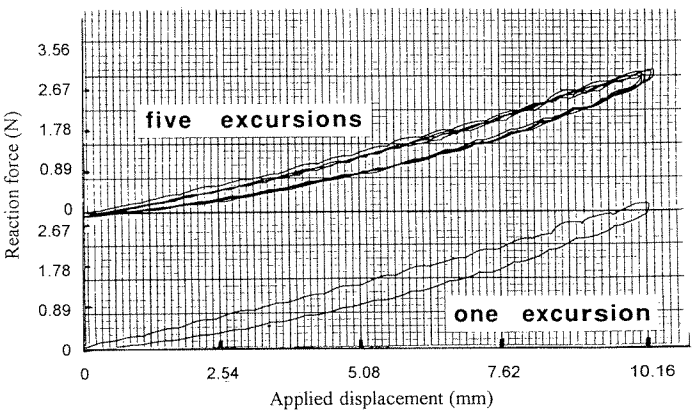

Figure 7.
Displacement-force records for one and five excursions. In the five-excursions plot, the curve which appears to be slightly higher is fourth excursion (the subject moved slightly), not the first. These records are from pilot testing in which a sixty second rest period was not used. However, the threaded rod driving the indentor tip was turned by hand; thus the applied indentation was still not fully continuous. Instead, the indentor was motionless for short periods of time (~0.5 second). During these short periods stress relaxation occurred; visible as a number of small dips and spikes.

minor changes in posture and muscle contraction strategies by the subject caused variations in the shape and, presumably, the stiffness of the muscle belly. Apart from this random variation, however, the response does not appear to exhibit a preconditioning effect. To test the qualitative observation regarding preconditioning, the data were also quantitatively examined. A second-order polynomial was fit through all the ascending data for each test. Data sets for each subcurve were then tested against this complete curve. Again, note that each complete displacement-force curve was actually made up from a number of separate subcurves, one for each tip. If a preconditioning effect were occurring, one would expect subsequent subcurves not to line up with the first subcurve, but to be shifted right: toward higher displacement (**Figure 8**). Thus, if preconditioning were occurring, one would expect the first data point for each subcurve to be below the complete curve, and the last to be above.

To detect this behavior, a statistical test was performed on the ascending data for each test. The deviations of the first and last data points of each subcurve from the complete curve were calculated. If the last data point for a given subcurve was above the complete curve, that deviation was given a positive sign. A positive sign was also given if the deviation for a first data point was below the complete curve. Otherwise, the deviation was given a negative value. Seventy-eight data points were available. This analysis found that the average of the deviations from the complete curve was between 0.076 and −0.081 N with 99 percent confidence; a negligible amount in this context. Thus, the tissue exhibits no preconditioning effect under these loads.

Twenty-minute Stress Relaxation Tests

Stress relaxation was less than 10 percent, with at least 90 percent confidence, at all times from 5 to 1,200 seconds (**Figure 9**). In informally monitoring the output of the load cell, it was observed that the majority of stress relaxation was completed within 1 second of the end of indentation.

Hysteresis Tests

The amount of hysteresis was essentially constant across rest times from 5 to 60 seconds (**Table 2**). Hysteresis was always present in the tissue's response. Examination of the data from displacement-force tests showed that the hysteresis was always $\leq$10 percent of the peak reaction force attained in all tests where that peak did not exceed 7.0 N.

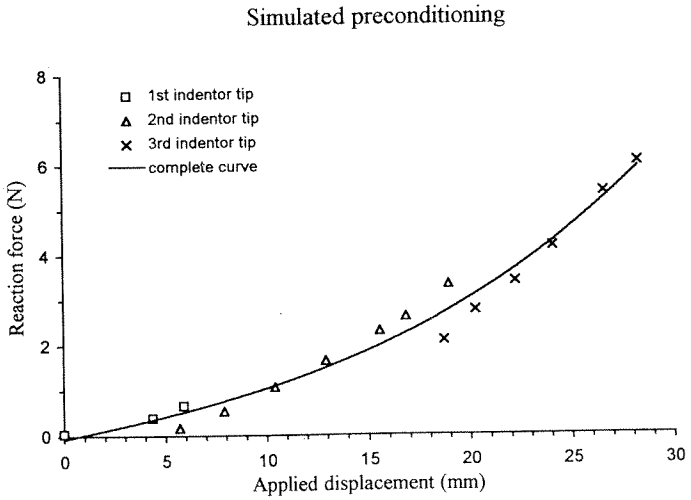

Figure 8.
Simulated preconditioning. This artificial set of data illustrates how the response of the tissue might appear if preconditioning were occurring. Note that the first data point of each subcurve is below the complete curve; and that the last data point of each subcurve is above the complete curve. This graph may be compared to the actual response of the tissue (**Figure 3**).

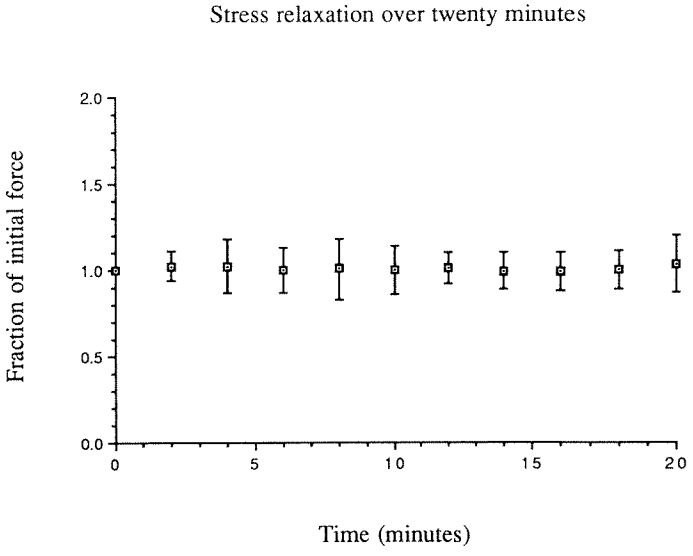

Figure 9.
Stress relaxation over 20 minutes. The data are from six tests, using various locations and both 8 and 19 mm diameter indentors. The error bars are $\pm$2 standard deviations; the reaction force reading at 5 seconds was taken as the initial value, thus no error bars at this point.

Table 2.
Hysteresis tests.

Delay before taking force reading	Change (N)	
5 seconds	average	3.45
	S.D.	0.11
10 seconds	average	3.42
	S.D.	0.09
30 seconds	average	3.43
	S.D.	0.11
60 seconds	average	3.46
	S.D.	0.10

The applied displacement was cycled back and forth between 7.9 and 12.8 mm; the difference in reaction forces is tabulated here. The differences were the same whether the applied displacement was increasing or dereasing and so are not shown separately.

Multisubject Tests

The displacement necessary to achieve 7.0 N reaction force averaged 21.2 mm for the relaxed cases and 18.25 mm for the mild exertion cases. The stiffness (slope of the displacement-force curve) at 7.0 N reaction force averaged 0.519 N/mm (relaxed), and 0.769 N/mm (mild exertion). Neither of these differences was statistically significant at high levels of confidence. Typically, the stiffness varied by a factor of three across the set of subjects (30).

Finite Element Modeling

Linear

The results of the linear cases are given in **Table 3.**

The displacement-force stiffnesses are roughly equal at ports II, III, and IV. The calculated displacement-force stiffness at port V is 23 percent lower than the average stiffness at the other ports. The data show that the displacement-force stiffness differences measured in the experimental tests are not simply a result of the geometry of the leg. There is no statistical correlation between the order predicted by the finite element modeling (**Table 2**) and that experimentally measured for either the relaxed or active muscle bellies (**Figure 10**); in fact, there is a slight negative correlation. Using a *t*-test on the experimental data for active muscle, we conclude that the displacement necessary to generate 6 N reaction force at port II (low stiffness) is greater that than at port V (high stiffness) with 99 percent certainty. The hypothesis that, using a homogeneous material assumption, the geometry of the leg and the port locations will predict the relative stiffnesses at the various locations is therefore not substantiated.

Table 3.
Calculated displacement-force stiffnesses at ports from linear cases.

Port	Displacement-force Stiffness (N/mm)
2 (full model)	0.263
3 (full model)	0.274
3 (top half model)	0.137
3 (bottom half model)	0.132
4 (full model)	0.276
5 (full model)	0.208

These linear models all used an elastic modulus of 0.00206 GPa (the linear portion of the stiffness estimate derived in the non-linear analysis).

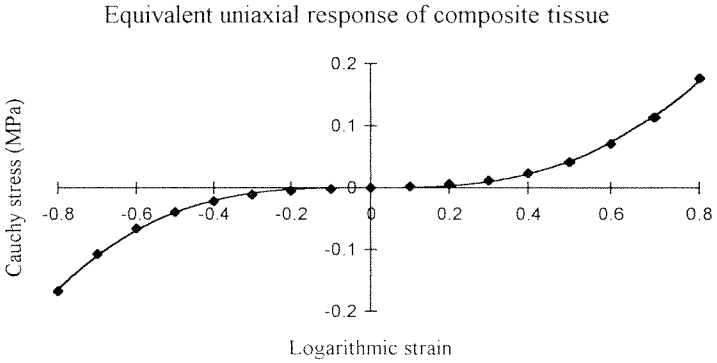

Figure 10.
Equivalent uniaxial response of composite tissue with strain energy constants c_{10} 0.0026 MPa, c_{11} 0.0057 MPa ($c_{01}=c_{10}/4.0$ assumed).

Nonlinear

Using the Jamus-Green-Simpson material formulation, the constants which best matched the response of the active and relaxed muscle cases at port III were c_{10}=0.0026 MPa, $c_{01}=c_{10}/4$=0.00064 MPa, c_{11}=0.0057 MPa ($c_{01}=c_{10}/4$ is a customary assumption (32,33); further, c_{01} is not a sensitive parameter). These constants were chosen by trial and error, based on comparison of the finite element analysis versus the experimental data (**Figure 11**). It should be noted here that it was also possible to fit the data nearly as well using the pair of constants c_{10} and c_{20}, or the pair of c_{10} and c_{30}; there is no strong basis for choosing the pair c_{10} and c_{11}. The equivalent uniaxial response of this material is nonlinear, as shown in **Figure 10.**

Magnified views (**Figure 12**) allow examination of the element distortion occurring in the strain concentra-

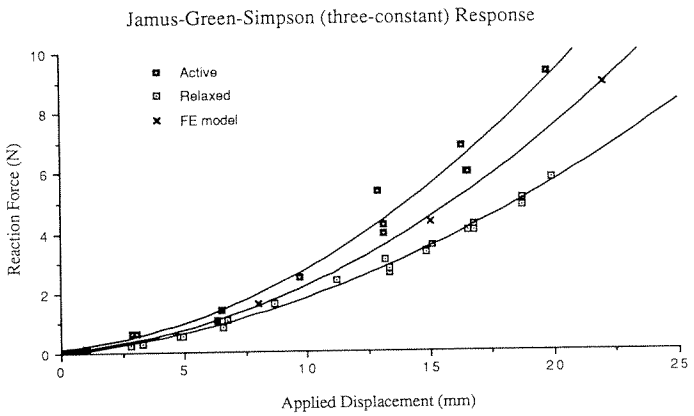

Figure 11.
Experimental data versus results of finite element model. Material constants for finite element model were chosen in order to achieve the best fit (subjectively judged) to the experimental data. In this case, the data was for the 'average' stiffness port, III. The constants were c_{10} 0.0026 MPa, $c_{01}=c_{10}/4=0.00064$ MPa, $c_{11}=0.0057$ MPa. These values are for this specific location only; the analysis showed significant variations in material stiffness with location.

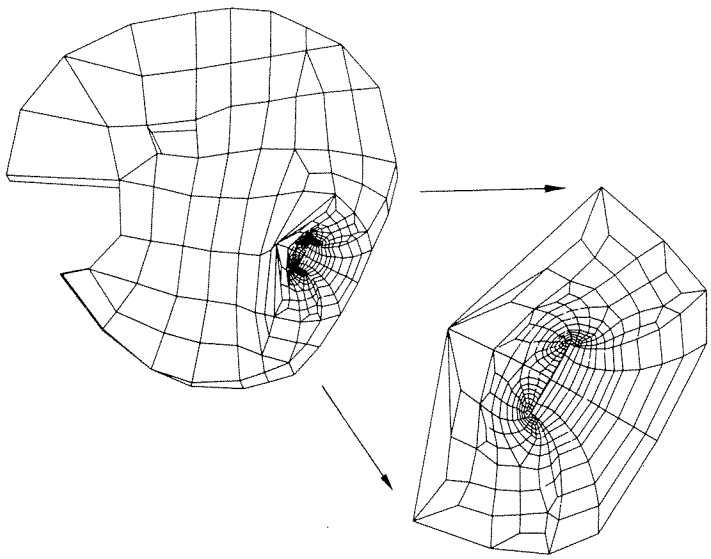

Figure 12.
Distorted element shapes about the indentor tip. Top view of a layer of elements, with magnified view of area of indentation showing high distortion about edge of the indentor tip.

tion about the edge of the indentor tip. Note that the distortion of the elements is less severe than that which occurred in the elastomeric disk model used to verify the adequacy of the mesh refinement (presumably because the tissue had a more nonlinear stiffness than did the elastomer). Severity of distortion is related to model instability and artificial stiffening; thus, the mesh refinement in this area is adequate (36,37).

DISCUSSION

The purpose of the study was to provide quantitative description of the nonlinear material stiffness and viscoelasticity occurring in the response of bulk muscular tissue, under loads such that these descriptions would apply to analyses of soft tissue support.

Direct comparison between the material stiffnesses calculated here and those reported earlier is difficult due to the difference in calculation methods (i.e., nonlinear versus linear). The initial stiffness calculated here is equivalent to 0.00206 MPa. At 0.137 MPa applied stress (the average stress under 7N applied to an 8 mm diameter indentor), the tangent stiffness is 0.600 MPa. These stiffnesses bracket those reported in the previous linear studies [0.021 to 0.195 MPa (6); 0.0062 to 0.109 MPa (13,26); 0.06 MPa (14); 0.05 to 0.145 MPa (16); 0.053 to 0.141 MPa (38)].

The average increase in stiffness with muscle activity was 48 percent; this is similar to results recently reported by Mak et al. (6). When a layer of skin was added to the model, the calculated stiffness of the remaining soft tissue dropped 23 percent: $c_{10}=0.0020$ MPa, $c_{01}=c_{10}/4=0.00049$ MPa, $c_{11}=0.0044$ MPa (30).

The detailed geometric modeling method used in this study may produce more accurate material calculations than those previously reported. The global and local geometry of the tissue was modeled in detail. A number of previous investigations have assumed uniaxial compression, which implicitly assumes that only the material directly under the indentor is physically present; stiffnesses calculated using this method probably represent an upper bound (12,13,16,26,38). Earlier work by Steege et al. modeled indentation by forcing displacement of a single node of the model, rather than a refined area of the mesh (14,15). Thus, while the global deformation was modeled, the local deformation about the indentation was not. The shape of the indentation occurring in the model was strongly influenced by the mesh and shape function of the elements local to the area. Mak et al. assumed indentation into an infinite half-space of tissue (6). In some sense, the converse of the finite element based model reported by Steege et al., the half-space solution was capable of modeling the deformation local to the

indentor but, because it models the limb as a half-space, could not model the global deformation of the limb.

Continuing stress relaxation and preconditioning were negligible, in strong contrast to the behavior reported for other soft tissues, such as tendon/ligament (2,3), articular cartilage (1,4), and human skin (24,25). Under an indentor at physiologic stress levels, articular cartilage exhibited a 600 to 1,800 second creep reponse (1). Conversely, in the present study, negligible stress relaxation was observed in the period between 5 and 1,200 seconds after indentation. It was informally observed that the majority of stress relaxation occurred within 1 second after the indentor tip stopped moving. Mak et al. have reported similar results for lower limb bulk muscular tissues (6); over 90 percent of the stress relaxation was completed within 2 seconds. At the load levels imposed, the composite tissue did not exhibit an observable preconditioning effect. Other reports of *in vivo* indentation studies of bulk muscular tissue have not reported on the absence or presence of preconditioning.

This short-term stress relaxation was also evidenced by the consistent presence of hysteresis. The amount of hysteresis recorded remained constant over rest times from 5 to 60 seconds, implying that it occurred in under 5 seconds (note, therefore, that the 60-second rest time used in the displacement-force tests was overly conservative). At higher loads (>12.0 N on the 8 mm indentor), significant continuing stress relaxation was observed, as well as greater hysteresis. These inelasticities were always accompanied by minor tissue damage (although the converse was *not* true; it was common to observe a small welt after testing in which increased inelasticity was not observed). The inflammation accompanying loading high enough to cause increased inelasticity was longer lasting (6–48 hours duration), and occasionally caused discoloration. It is difficult to place the exact process of this inflammation within the physiologic mechanisms discussed in the investigation of pressure sores. However, the occurrence of this tissue damage did appear to be a hallmark of increased inelastic response in the tissue. Thus, it is possible that below 7.0 N the inelasticity was due to intrinsic viscoelasticity and/or interstitial fluid flow, while the increased inelasticity seen at higher loads reflects breakdown of the structural elements within the tissue.

Application of these data to soft tissue support problems is hindered because non-amputated limbs were tested, and because a full range of stress histories was not applied. No residua were tested in the present work. This limitation was accepted in order to allow use of distortions presumed to be higher than those experienced by a prosthetic socket wearer. Greater inelasticity is observed at higher loads (speaking in general terms) with this tissue; thus, the limitation allows the present work to provide an upper bound on the inelasticities which might be expected. The differences and similarities in mechanical behavior between residual and non-amputated limbs have been discussed by other investigators (6). The indentor imposed a stress field on the material that was high in shear stress and low in hydrostatic stress. The stress field in the residuum within a loaded prosthetic socket has, in general, lower shear and higher hydrostatic stresses. This study did not evaluate the effect of variations in the hydrostatic stress on the shear stiffness of the tissue. The fact that the indentations were used (i.e., rather than a stress field more similar to that occurring in a socket) is a limiting factor in applying these data. While the tissue constants replicate the tissue behavior under indentation, their performance under other modes of deformation was not examined.

The results are encouraging in that they imply that a hypoelastic assumption (single-valued stress-stretch relationship) may be a reasonable first approximation for this tissue's quasi-static response; at least under loads relevant to the design of soft tissue support systems. The material model/finite element formulation used is available in an increasing number of commercial finite element packages; thus, its implementation in modeling soft tissue support need not be laborious. The present study found that the stiffness nonlinearity requires the use of higher-order terms in the strain energy function (in the present study, the c_{11} term was included), rather than the two terms (Mooney-Rivlin formulation) traditionally used (31,33). This observation was also reported for modeling of passive myocardium in biaxial tension by Nielsen, Hunter, and Smaill (39).

Development of an *in vivo* method for determining the geometry and stiffness of the soft tissues within an artificial limb is clearly an important goal in the progress of CAD/CAM methods of prosthetic socket production. An hypothesis of the present study was that, using a refined geometric model, the geometry of the tissue would explain a significant portion of the experimentally measured difference in stiffness between the ports. Again, the data show that this hypothesis is rejected. The assumption that the tissue may be treated as one homogeneous material, therefore, has significant limitations. Thus, a system which records the limb's

internal geometry and a semi-quantitative description of the stiffness, such as the ultrasonic elastography system being developed for early detection of tumors, might be a valuable resource (40).

CONCLUSIONS

The displacement-force response for this composite tissue always exhibited hysteresis. The composite tissue relaxed less than 10 percent under stress in the time period between 5 and 1,200 seconds after indentation. Stress relaxation was informally observed at shorter time periods, particularly within the first second after indentation, but was not quantified in this study. It was not necessary to precondition the tissue to observe a repeatable displacement-force response. These characterizations of the tissue's response are based on tests using 0.0 to 7.0 N applied to an 8.0 mm diameter flat-tipped indentor. At higher loads (>12.0 N), the tissue began to exhibit more inelastic response (stress relaxation which continued beyond 5 seconds, preconditioning effect, increased hysteresis), accompanied by tissue damage.

The typical composite tissue stiffness could be represented, using the Jamus-Green-Simpson strain energy formulation for elastomers, as:

$$c_{10} = 0.0026 \text{ MPa}, c_{11} =$$

$$0.0057 \text{ MPa } (c_{01} = c_{10}/4.0 \text{ assumed}).$$

This stiffness corresponds to an initial elastic modulus of 0.02 MPa (3.0 psi). For tests in which a single subject was tested in a variety of locations, the composite tissue stiffness varied by a factor of two. For tests in which a number of subjects were tested in the same anatomic location, the composite tissue stiffness varied by one part in three.

In spite of detailed modeling of the geometry of the leg and of the deformation, the model (using a homogeneous material assumption) was unable to account for the displacement-force stiffness differences experimentally recorded at various locations on the leg. For this composite tissue, therefore, the homogeneous material assumption has significant limitations.

ACKNOWLEDGMENTS

The authors gratefully acknowledge the support of the National Institutes on Disability and Rehabilitation Research and of the New England Medical Center Hospitals, as well as the valuable comments of the reviewers.

REFERENCES

1. Hayes WC, Mockros LF. Viscoelastic properties of human articular cartilage. J Appl Physiol 1971:3:562–8.
2. Viidik A. Interdependence between structure and function in collagenous tissues. In: Viidik A, Vaust J, eds. Biology of collagen. New York: Academic Press, 1972:257–80.
3. Fung YC. Biomechanics: mechanical properties of living tissues. New York: Springer-Verlag, 1981.
4. Mow VC, Hou JS, Owens JM, Ratcliffe A. Biphasic and quasilinear viscoelastic theories for hydrated soft tissues. In: Mow VC, Ratcliffe A, Woo SL, eds. Biomechanics of diarthrodial joints. Vol. I. New York: Springer-Verlag, 1990.
5. Sanders JE, Daly CH. Normal and shear stresses on a residual limb in a prosthetic socket during ambulation: comparison of finite element results with experimental measurements. J Rehabil Res Dev 1993:30:191–204.
6. Mak AFT, Liu GHW, Lee SY. Biomechanical assessment of below-knee residual limb tissue. J Rehabil Res Dev 1994:31:188–98.
7. Todd BA, Thacker JG. Three-dimensional computer model of the human buttocks, in vivo. J Rehabil Res Dev, 1994:31:111–9.
8. Vlasov VZ, Leontev NN. Beams, plates and shells on elastic foundations. English translation in: NASA TT F 357. Springfield, VA: Clearing House for Federal Scientific and Technical Information, 1960.
9. Murphy EF. Transferring load to flesh. Part I. Concepts. Bull Prosthet Res 1971:Fall:38–61.
10. Bennett L. Transferring load to flesh. Part II. Analysis of compressive stress. Bull Prosthet Res 1971:Fall:45–63.
11. Chow WW, Odell EI. Deformations and stresses in soft body tissues of a sitting person. J Biomech Eng 1978:100:79–87.
12. Nakamura S, Crowninshield RD, Cooper RR. An analysis of soft tissue loading in the foot: a preliminary report. Bull Prosthet Res 1981:18:27–34
13. Krouskop TA, Muilenberg AL, Dougherty DR, Winningham DJ. Computer-aided design of a prosthetic socket for an above-knee amputee. J Rehabil Res Dev 1987:24(2):31–8.
14. Steege JW, Schnur DS, Childress DS. Finite element prediction of pressure at the below-knee socket interface. In: Biomechanics of normal and prosthetic gait. New York: ASME, 1987:BED-4:39–44.
15. Steege JW, Childress DS. Finite element modelling of the below-knee socket and limb: Phase II. In: Modelling and contol issues in biomechanical systems. New York: ASME, 1988:BED-4:121–9.
16. Reynolds D. Shape design and interface load analysis for below-knee prosthetic sockets (PhD thesis). London: University of London, 1988.
17. Chung KC, McLaurin CA, Brubaker CE, Brienza DM, Sposato BA. A computer-aided shape sensing system for

custom seat contours. In: Proceedings of the 13th Annual RESNA Conference; 1990, Washington, DC. Washington, DC: RESNA Press, 1990:395–6.

18. McMahon TA. Muscle mechanics. In: Skalak R, Chein S, eds. Handbook of bioengineering. New York: McGraw-Hill, 1987: 7:1–26.
19. Bogen DK. Strain energy descriptions of biological swelling, I & II: single & multiple fluid compartment models. J Biomech Eng 1987:109:252–62.
20. Horowitz A, Sheinman I, Lanir Y. Non-linear incompressible finite element for simulated loading of cardiac tissue—part II: 3D formulation for thick ventricular wall segments. J Biomech Eng 1988:110:62–8.
21. Humphrey JD, Yin FCP. On constitutive relations and finite deformations of passive cardiac tissue: I. Pseudostrain-energy function. J Biomech Eng 1987:109:298–304.
22. Hunter PJ, McCulloch AD, Nielsen PMF, Smaill BH. A finite element model of passive ventricular mechanics. In: Spilker RL, Simon BR, eds. Computational methods in bioengineering. New York: ASME, 1988:493–503.
23. Spilker RL, Suh J-K, Vermilyea ME, Maxian TA. Alternate hybrid, mixed, and penalty finite element formulations for the biphasic model of soft hydrated tissues. In: Mow VC, Ratcliffe A, Woo SL, eds. Biomechanics of diarthrodial joints. Vol I. New York: Springer-Verlag, 1990:215–435.
24. Oomens CWJ, van Campen DH, Grootenboer HJ. In vitro compression of a soft tissue layer on a rigid foundation. J Biomech 1987:20:923–35.
25. Manschot JFM, Brakkee AJM. The measurement and modelling of the mechanical properties of human skin in vivo I & II. J Biomech 1986:19:511–21
26. Krouskop TA, Dougherty DR, Vinson FS. A pulsed Doppler ultrasonic system for making noninvasive measurements of the mechanical properties of soft tissues. J Rehabil Res Dev 1987:24(2):1–8.
27. Reger SI, Navarro RR, Neth DC. Computerized shape reproduction for custom contoured wheelchair seating systems. J Rehabil Res Dev 1990:28:(Suppl):467–8.
28. Sposato BS, Chung KC, McLaurin CA, Brubaker CE, Brienza DM. Prescribing customized contoured seat cushions by computer-aided shape sensing. In: Proceedings of the 13th Annual RESNA Conference; 1990, Washington, DC. Washington, DC: RESNA Press, 1990:103–4.
29. Lebedev NN, Ufliand IA. Axisymmetric contact problem for an elastic layer. PMM 1958:22:442–50.
30. Vannah WM. Indentor tests and finite element modelling of bulk muscular tissue in vivo (Dissertation). Evanston, IL: Northwestern University, 1990.
31. Nagtegaal JC. On analysis of elastomeric materials. In: Marc background papers. Vol. F, ch 15. Palo Alto, CA: Marc Analysis Research Corp., 1988.
32. Oden JT. Finite elements of nonlinear continua. New York: McGraw-Hill. 1972:ch 15–18.
33. Ogden RW. Elastic deformations of rubberlike solids. In: Hopkins HG, Sewall MJ, eds. Mechanics of solids: the Rodney Hill 60th anniversary volume. Oxford: Pergamon Press, 1982:499–537.
34. Press WH, Flannery BP, Teukolsky SA, Vetterling WT. Numerical recipes in C: the art of scientific computing. Cambridge: Cambridge University Press, 1988:528–39.
35. Herrmann LR. Elasticity equations for incompressible and nearly incompressible materials by a variational theorem. AIAA J, 1965:3:1896–900.
36. Hughes TJR. The finite element method. Englewood Cliffs, NJ: Prentice-Hall, 1987:ch 4.
37. Malkus DS. Advanced topics in the theory of mixed and penalty methods: pressure modes and error estimates. In: Hughes TJR, ed. The finite element method. Englewood Cliffs, NJ: Prentice-Hall, 1987:276–303.
38. Malinauskas M, Krouskop TA, Barry PA. Noninvasive measurement of the stiffness of tissue in the above-knee amputation limb. J Rehabil Res Dev 1989:26(3):45–52.
39. Nielsen PMF, Hunter PJ, Smaill BH. Biaxial testing of membrane biomaterials: testing equipment and procedures. J Biomech Eng 1991:113:295–300.
40. Cespedes I, Ophir J, Ponnekanti H, Maklad N. Elastography: elasticity imaging using ultrasound with application to muscle and breast in vivo. Ultrason Imaging 1993:15:73–88.